

Size Effects in Formation of Segregation and Grain-Boundary Decomposition in Nanocrystalline Alloys

I. K. Razumov

Institute of Metal Physics, Ural Branch, Russian Academy of Sciences, Yekaterinburg, 620041 Russia

e-mail: rik@imp.uran.ru

Received September 7, 2017

Abstract—The effect of finite grain size on the formation of grain boundary segregations, and on the morphology of precipitates during decomposition, is studied. It is shown that in dilute solid solutions there are critical grain sizes at which decomposition is suppressed, both at the grain boundaries and in the bulk. A generalized phase-equilibrium diagram is constructed that considers the size factor, and a classification of the morphologies of precipitates during grain-boundary decomposition is suggested.

Keywords: nanocrystalline alloys, grain size, grain-boundary decomposition, spinodal decomposition, segregation, pseudospinodal line

DOI: 10.1134/S0036024418070233

INTRODUCTION

Grain size affects the durability, plasticity, fragility, and impact strength of steels and alloys [1, 2]. As a rule, the properties of a material are greatly enhanced upon the transition to the nanostructured state [3], which can be induced by, e.g., intense plastic deformation [4]. The production of steels with a nanograin structure is now a promising field [5]; combining plastic deformation with brief annealing, we can obtain steel with grain sizes of 20–200 nm [6–8].

Multicomponent systems offer broad opportunities for designing new materials [9–11]. The chemical potential of impurity atoms differs at a grain boundary (GB) and in the bulk, so the traditional phase diagrams for the nanocrystalline state are applicable only locally [12]. Segregations at the grain boundaries affect the initial conditions and morphologies of precipitates during grain-boundary decomposition, which finds important practical applications in, e.g., dispersion hardening and the stabilizing of grain structure [13, 14] (the precipitation of fine particles of Nb, V, and Ti carbides and nitrides at GBs during the production of steels [15, 16]). Despite the seeming simplicity of the topic, the role of the size factor in the development of grain-boundary decomposition and segregation remains poorly studied, and the relevant data have not been dealt with systematically in the literature.

The size effects in the development of GB segregations in an ideal solid solution were considered in [17], and formulas for the critical grain sizes at which the nature of segregations and the bulk properties of a material change qualitatively were obtained. In this

work, we apply these concepts to nonideal solid solutions and alloys subjected to decomposition. A classification of the decomposition morphologies of nanocrystalline alloys is proposed that depends on the grain size and the position of the alloy parameters on a generalized phase-equilibrium diagram.

RESULTS AND DISCUSSION

Suppression of Grain-Boundary Decomposition in the Nanocrystalline State

The free-energy density of a binary alloy in the approximation of a regular solution has the form [18]

$$f(c) = \varepsilon c + (1/2)\nu c^2 + kT [c \ln c + (1 - c) \ln(1 - c)], \quad (1)$$

where c is the concentration of component, ε and ν are the energies of dissolution and mixing of impurity; $\nu = \sum_n z_n v_n$; z_n is the number of neighbors in the n th coordination sphere; and v_n is the effective interaction between the impurity atoms in the n th coordination sphere.

Let us examine a grain in the form of a sphere with radius L and boundary layer width d , and the formation of precipitates of a new phase can occur at the grain boundary (Fig. 1). When equilibrium is reached, the concentrations of the impurity in a GB and in the volume of each phase are related by the condition of the equality of chemical potentials; i.e., $\mu_{GB} = \mu_{b(p)}$, where $\mu = \delta f / \delta c$, from which the Fowler equation follows [19]. In addition, the size dependence of the con-

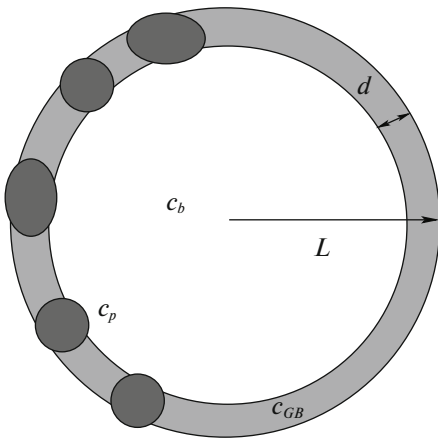


Fig. 1. Grain in the form of a sphere with radius L and having a boundary layer with width d ; concentrations c_b , c_{GB} , and c_p are achieved in the grain volume, at its boundary, and in the precipitates of the new phase, respectively, upon reaching equilibrium.

centration distribution obeys the law of the conservation of matter. Therefore,

$$\frac{c_{GB}}{(1 - c_{GB})} = \frac{c_b}{(1 - c_b)} \exp \left[\frac{\delta \varepsilon_b + v(c_b - c_{GB})}{kT} \right], \quad (2)$$

$$\delta \varepsilon_s = \varepsilon_b - \varepsilon_{GB},$$

$$\frac{c_{GB}}{(1 - c_{GB})} = \frac{c_p}{(1 - c_p)} \exp \left[\frac{\delta \varepsilon_p + v(c_p - c_{GB})}{kT} \right], \quad (3)$$

$$\delta \varepsilon_p = \varepsilon_p - \varepsilon_{GB},$$

$$(\tilde{L} - 1)^3 c_b + (\tilde{L}^3 - (\tilde{L} - 1)^3) \times (c_{GB}(1 - \tilde{V}_p) + \tilde{V}_p c_p) = \tilde{L}^3 c_0, \quad (4)$$

where ε_{GB} , ε_b , and ε_p are the energy of dissolution of impurity at a GB, in the grain volume, and in the precipitates, respectively; c_{GB} , c_b , and c_p are the corresponding concentrations of the impurity; c_0 is the average concentration of the impurity over the sample; $\tilde{L} = L/d$ is the relative grain size; \tilde{V}_p is the fraction of the surface layer occupied by the new phase; $\tilde{V}_p = V_p / (4\pi[L^3 - (L - d)^3]/3) = S_p/S_{GB}$, where S_p and S_{GB} are the surface area of a grain occupied by the precipitates of the new phase and the remaining surface area; V_p is the volume occupied by the new phase. For simplicity, it is assumed that the energy of mixing is the same everywhere; i.e., $v_{GB} = v_b = v_p = v$. Equations (2)–(4) contain four unknowns (c_{GB} , c_b , c_p , and \tilde{V}_p). In describing decomposition in two-phase systems, the condition of a

common tangent to the free-energy minima is applied as an additional equation [18]:

$$\mu_{GB} = \mu_p = \frac{f_p(c_p) - f_{GB}(c_{GB})}{c_p - c_{GB}}, \quad (5)$$

where $f_p(c_p)$ and $f_{GB}(c_{GB})$ are the free energies in the precipitate and on the rest of the GB surface, which are calculated using Eq. (1) at $\varepsilon = \varepsilon_p$ and $\varepsilon = \varepsilon_{GB}$, respectively.

Grain-boundary decomposition in doped steels usually involves carbides, e.g., NbC and VC. Herewith, Nb(V) atoms show no pronounced tendency toward attraction in pure Fe, and precipitates form due to the gain in energy upon the formation of carbide. Assuming that carbon is present in sufficient amounts, we can still speak of the effective attraction of impurity atoms ($v \sim -1$ eV/at). Typical energies of segregation are $\delta \varepsilon_s \sim 0.2$ eV/at. We also assume for simplicity that the energy of dissolution does not vary along the boundary; i.e., $\delta \varepsilon_p = 0$. It is in this case easy to verify by substituting Eq. (1) into Eq. (5) that the solution does not depend on the ε_{GB} value. Typical concentrations of doping additives are around $c_0 \sim 0.001$, and the width of the boundary can be estimated as $d \sim 1$ nm. These figures allow us to parametrize the set of Eqs. (1)–(5) roughly, and to discuss the qualitative features of the solution.

The numerical solution in Fig. 2 shows that the fraction of the new phase at an S_p/S_{GB} grain boundary shrinks linearly along with grain size L . In addition, there is a critical grain size at which the S_p/S_{GB} value vanishes because the impurity content in the alloy is insufficient for reaching the decomposition threshold at the boundary. Grain-boundary decomposition can thus be completely suppressed in the nanocrystalline state.

Complete Removal of an Impurity from the Grain Volume in Dilute Solid Solution

Let us examine the size effects when grain-boundary segregations form in the absence of new phase precipitates (this is possible in solid solutions that are close to ideal and in such mixed systems as γ Fe–Ni, α Fe–Mo, and γ Fe–Mn alloys, where $v \geq 0$). The set of Eqs. (2)–(5) is in this case reduced to Eqs. (2) and (4), and $\tilde{V}_p = 0$. It was shown in [17, 20] that the grain volume is ideally cleansed of the impurity upon reaching the critical grain size even in an ideal solid solution, and the concentration at the grain boundary becomes dependent on the size. These effects are most pronounced at impurity concentrations of at least one percent, ambient (room) temperatures, and long times of exposure. In industry, steels are used that are up to 10% Ni, Cr, Mn, Mo, or Co, with V, Ti, Si, and other elements in smaller amounts. Herewith, typical ener-

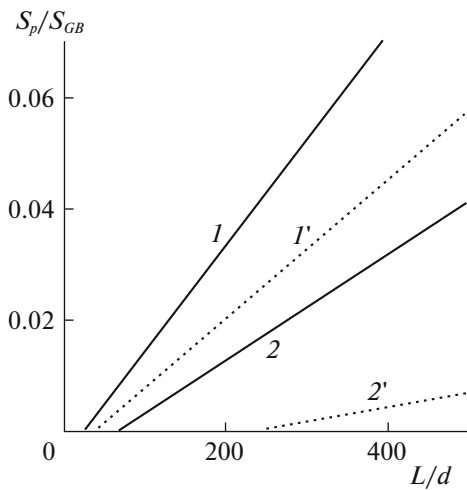


Fig. 2. Fraction of the grain boundary phase on a grain's surface, depending on the grain size upon reaching equilibrium under the conditions $\delta\epsilon_s = 0.2$ eV/at and $v = -1$ eV/at; $T = (1, 1')$ 1100 (2, 2') 1160 K; $c_0 = (1, 2)$ 0.0012 and $(1', 2')$ 0.001.

gies of mixing are $v = \pm 0.3$ eV/at [21, 22] and energies of segregation are around $\delta\epsilon_s \sim 0.3$ eV/at; Fe–Ni alloy is close to an ideal solid solution ($v \approx 0$) [23]. The formation of segregations in each system require special consideration (the dependence of energy parameters on concentrations; ordering tendencies; the precipitation of intermediate phases; and so on). Here we confine ourselves to a simple qualitative model that reproduces the general characteristic traits of phenomena without claiming accuracy of parametrization.

As seen from Fig. 3a, if the grain size falls to a critical value, its volume is ideally cleansed of the impurity. The critical size increases as average concentra-

tion c_0 falls and shrinks as value v rises. A comparison of Figs. 3b and 3a shows that exhaustion of the impurity in the bulk reduces grain-boundary concentration c_{GB} upon reaching a small grain size.

Size Effects in Spinodal Decomposition

Let us examine a thermodynamically unstable alloy ($v < 0$) in which spinodal decomposition (SD) starts upon cooling below the critical temperature. An example of such a system is Fe–Cu alloy. For simplicity, the classical models of decomposition [18, 24, 25] do not consider the dynamics of thermal fluctuations. The alloy in this case remains homogeneous in the region of the phase-equilibrium diagram between the binodal and spinodal lines, and decomposition begins instantaneously over the volume of the material by a mechanism of the escalation of infinitesimal long-wave fluctuations when cooled below spinodal temperature T_s . If the fluctuations in the volume grow slowly, discontinuous decomposition begins first at the grain boundary, producing a regular morphology of precipitates in a wide near-boundary layer [26]. Typical SD patterns are shown in Fig. 4, which we obtained in [12, 26] with a tendency toward the segregation of one component at GBs (Fig. 4a), and with an increase in the diffusion coefficient at GBs relative to the bulk (Figs. 4b, 4c).

Unlike mean-field models, a Monte Carlo (MC) simulation automatically considers thermal fluctuations in a composition and makes the kinetics of decomposition more complex. The classical spinodal in the phase-equilibrium diagram of the alloy disappears [27], and the $c(T_{ps})$ pseudospinodal curve separating the regions of homogeneous and heterogeneous nucleation emerges in place of it [28]. At slight undercooling below T_{ps} , the decomposition develops homo-

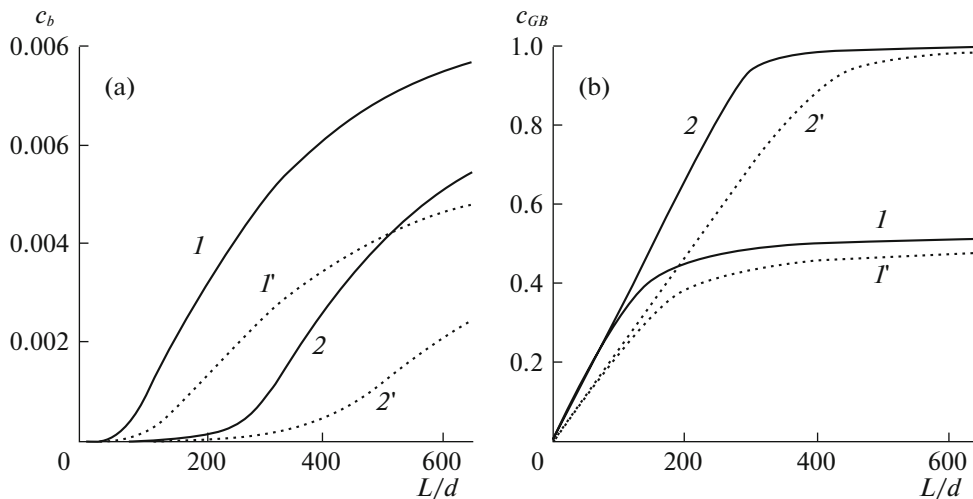


Fig. 3. Dependences of the equilibrium concentration of an impurity (a) in a grain's volume and (b) at its boundary on the grain size under the conditions $\delta\epsilon_s = 0.3$ eV/at; $T = 350$ K; $v = (1, 1')$ 0.3 and $(2, 2')$ 0 eV/at; $c_0 = (1, 2)$ 0.01; $(1', 2')$ 0.007.

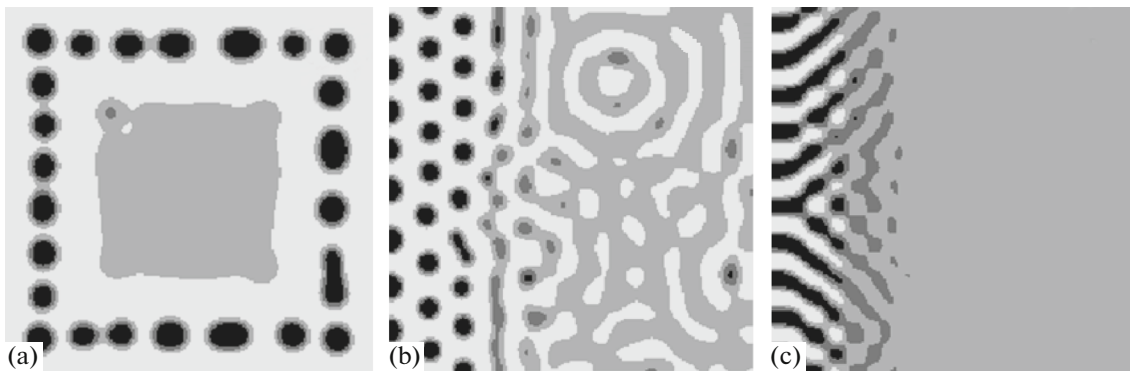


Fig. 4. Typical spinodal decomposition patterns (a) with a trend toward the segregation of one component at grain boundaries (coinciding with the boundaries of the square) and (b, c) upon the acceleration of diffusion at grain boundaries compared to the volume [12, 26] at $c_0 =$ (a, b) 0.3 and (c) 0.5.

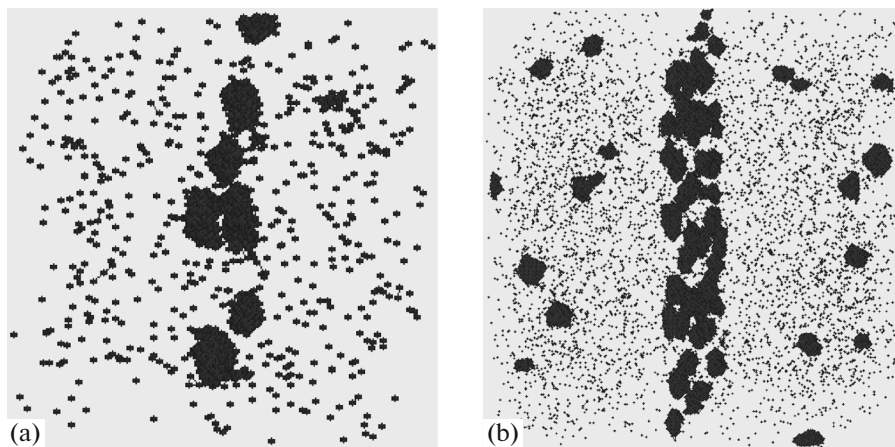


Fig. 5. Typical patterns of the decomposition of Fe–Cu alloy with the BCC lattice in cube with sizes of (a) $40 \times 40 \times 40$ and (b) $90 \times 90 \times 90$ elementary cells when the degree of decomposition $S = 0.20$. The grain boundary is represented by the plane passing through the cube's center: $c_0 = 0.012$ and $T = 700$ K; only Cu atoms are shown.

generously after an incubation period. In small grains, the impurity atoms have time to segregate at the boundaries, so their concentration in the grain volume falls below the $c(T_{ps})$ line. In this case, there is no decomposition in the bulk, and the precipitates of a new phase are located along the GBs. This effect was apparently observed recently in a Monte Carlo simulation of decomposition in Fe–Cu alloy [29].

The results from MC simulations of decomposition at different grain sizes are shown in Fig. 5. The simulation was performed for a sample in the form of a cube with periodic boundary conditions using the kinetic Monte Carlo method [30] with an effective Cu–Cu interaction potential of $\{-7.4, -2.3, -0.3\}$, as in [28]. This potential does not consider magnetic effects and has no concentration dependence, but it was sufficient for the aims of this work. It was assumed that a plane passes through the center of the sample, near which (in a layer with a width of 2 lattice parameters) the energy of copper segregation is $\delta\epsilon_s = 0.05$ eV/at, in

accordance with [29]. The plane thus imitates the grain boundary, while the grain size corresponds to the cube edge. As can be seen from Fig. 4, the decomposition in a small grain finishes with the formation of precipitates at the GB, while decomposition in grains with larger sizes develops both in the volume and at the grain boundary.

The evolution of the degree of decomposition in the volume for different grain sizes is shown in Fig. 6. A boundary region with a width of 10 lattice parameters was excluded from consideration in constructing these graphs, and the degree of decomposition was calculated using the formula

$$S = \frac{1}{N} \sum_{j=1}^N \theta \left(\frac{1}{Z} \sum_{k=1}^Z \sigma_k^{(j)} - q \right), \quad (6)$$

where N is the number of Cu atoms in the sample, $\sigma_k^{(j)}$ denotes the numbers of occupation for the nearest neighbors around the j th lattice site, $Z = 8$ is the coord-

dination number for the nearest neighbors in the BCC lattice, and $\theta(x)$ is the Heaviside function. According to Eq. (6), if the local concentration of Cu near the precipitate is not lower than q , a Cu atom is considered to belong to the precipitate. It was assumed in the calculations that $q = 0.8$.

As can be seen from the comparison of curve 1 (Fig. 6) constructed without the grain boundary with curves 2–5, the effect of the GB on the decomposition in the grain volume remains substantial for samples with sizes of $L/d \sim 50$. This effect is expressed through a slowing of decomposition at the initial stages due to an increase in the period of incubation within the grain volume, and in the accelerated transition to the evaporation–condensation stage, at which precipitates in the grain volume dissolve (and degree $S(n)$ of decomposition in the volume falls) as a result of the growth of precipitates at the GB.

The condition for decomposition in the grain volume in the first approximation takes the form

$$L > \sqrt{D\tau(c_0)}, \quad (7)$$

where $\tau(c_0)$ is the incubation period. Equation (7) shows that decomposition in the bulk is suppressed when the impurity atom can travel a distance of around the grain's radius and segregate at the GB in the time corresponding to the incubation period. To adjust Eq. (7), we may take into account that the concentration of the impurity in the grain volume deviates from the equilibrium concentration as a result of the development of segregations, due to which the period of incubation grows over time. In any case, MC simulation remains the only way of determining the $\tau(c)$ dependence.

Classifying Precipitate Morphologies with Allowance for Grain-Boundary Decomposition: Generalized Diagram of Alloy Phase States

The phase-equilibrium diagram of a regular solid solution model [18] contains two characteristic lines: binodal $c^e(T)$ and spinodal $c^{sp}(T)$. The binodal line corresponds to the equilibrium impurity concentration, and the spinodal line determines the condition for the loss of stability with respect to infinitesimal fluctuations in the composition. The classical spinodal line does not consider the finite amplitude of thermal fluctuations, so it is absent in MC simulations [27]. The $c^{ps}(T)$ pseudospinodal line, near which the incubation period of the homogeneous nucleation tends to infinity, can be introduced instead [28].

The presence of grain boundaries complicates this picture considerably. Effects associated with grain boundaries are not considered in the classical phase diagram, which remains valid in the local sense. In [12], it was proposed a generalized phase-equilibrium diagram in (T, c_0) coordinates, where c_0 is the mean

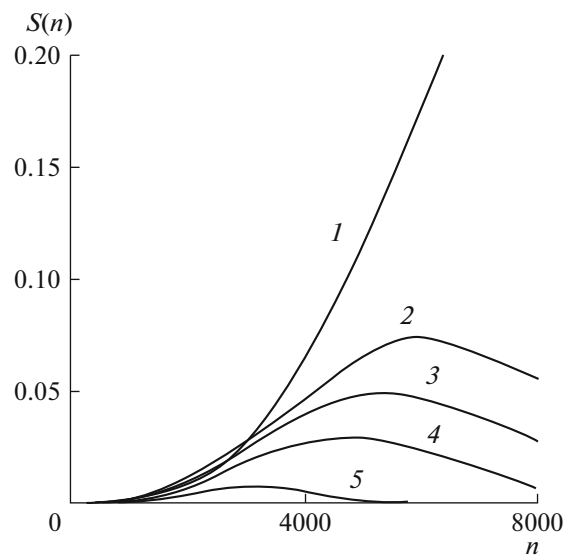


Fig. 6. Evolution of the degree of decomposition in the bulk as a function of the number of jumps per one impurity atom (I) in an infinite medium and at grain sizes L/d of (2) 45, (3) 40, (4) 35, and (5) 30; $c_0 = 0.012$ and $T = 700$ K. The near-boundary area is excluded from consideration.

composition of the alloy. This kind of diagram characterizes the phase state of the alloy as a whole, allowing us to consider the finite size effects.

Since decomposition is facilitated at a GB and suppressed in the grain volume, the lines $c^e(T)$ and $c^{ps}(T)$ of the classical diagram in the (T, c_0) coordinates are split for the boundary and the volume. Five regions of substantially different types of alloy behavior thus appear.

Using the expression for the free energy density Eq. (1), and in light of the condition of the equality of phase chemical potentials and the common tangent rule, we can obtain the familiar equation for the equilibrium solubility limit in a spatially homogeneous medium:

$$\frac{v}{2kT} = \frac{1}{1 - 2c_{\text{inf}}^e} \ln \left(\frac{c_{\text{inf}}^e}{1 - c_{\text{inf}}^e} \right). \quad (8)$$

Let us calculate the c_{inf}^e value from Eq. (8) and substitute it into Eqs. (2) and (4) in place of parameter c_{GB} . We then solve the resulting set with respect to parameters c_b and c_0 at $\tilde{V}_p = 0$ and take the obtained c_0 value as the $c_{GB}^e(T)$ value. The corresponding line of the generalized phase-equilibrium diagram determines the mean composition of the alloy at which grain-boundary decomposition becomes viable.

Let us substitute the c_{inf}^e value obtained from Eq. (8) into Eqs. (2) and (4) in place of the c_b value. We then solve the resulting set of equations with

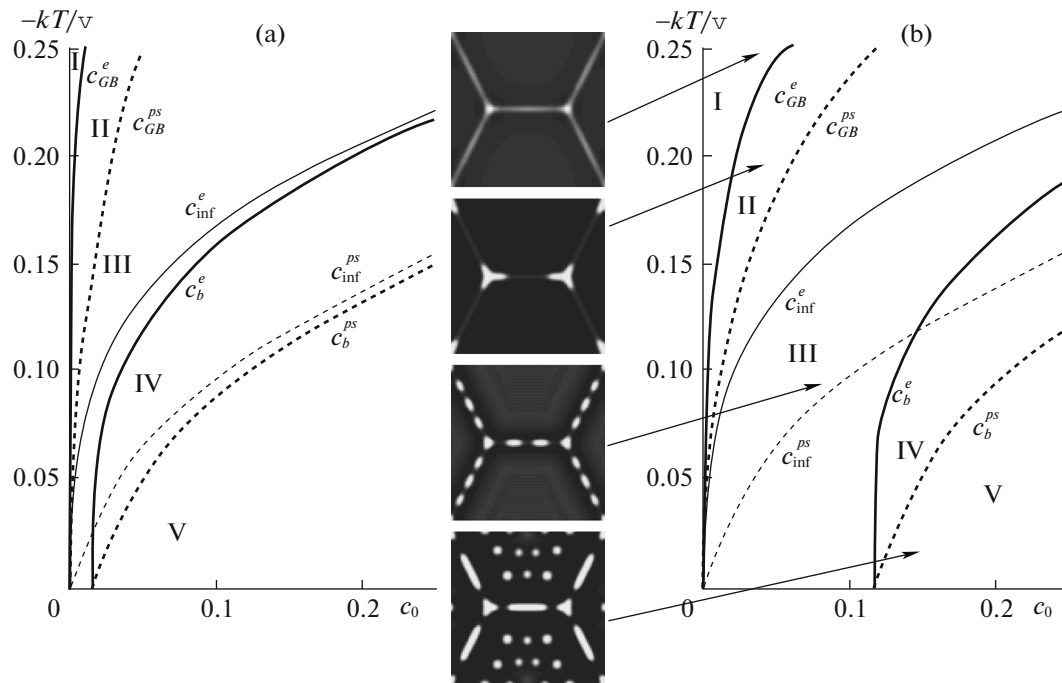


Fig. 7. Generalized diagrams of states of the alloy at (a) $L/d = 200$ and (b) $L/d = 25$; the $c_{GB(b,inf)}^e(T)$ phase-equilibrium lines were constructed using Eqs. (1)–(5) and (8) and the $c_{GB(b,inf)}^{ps}(T)$ pseudospinodal lines in qualitative agreement with them. The central column shows the morphologies of grain-boundary segregations and decomposition in the phase-field simulation for different regions of the diagram.

respect to the c_{GB} and c_0 values at $\tilde{V}_p = 0$ and take the obtained c_0 value as the $c_b^e(T)$ value. The new line of the generalized phase diagram determines the mean composition of the alloy at which the possibility of decomposition in the volume of grains exists even after the formation of GB segregations. Since the line is constructed at $\tilde{V}_p = 0$, we assume here that the grain-boundary decomposition with the generation of a new phase is either suppressed despite the emergence of segregations or did not have enough time to develop. Such a scenario is possible in particular because the formation of a new phase in real systems often requires reconstruction of the lattice, and grain-boundary decomposition can thus have its own incubation period after the formation of a segregation layer. Thus, the $c_b^e(T)$ line in nature is generally metastable; if grain-boundary decomposition starts simultaneously with the development of segregations, it loses its meaning.

At the moment, there are no theoretical models that allow us to adequately calculate the $c_{inf}^{ps}(T)$ pseudospinodal line. It was shown in [28] that the $c_{inf}^{ps}(T)$ value in an MC simulation differs considerably from the classical spinodal line. In this work, we limit ourselves to a schematic picture of the $c_{inf}^{ps}(T)$ curve.

A generalized diagram of the phase states for large and small grains is shown in Fig. 7. The $c_{GB}^e(T)$, $c_b^e(T)$, and $c_{inf}^e(T)$ lines were calculated using Eqs. (1)–(5) and Eq. (8), and the $c_{GB}^{ps}(T)$ and $c_b^{ps}(T)$ lines were drawn conditionally, i.e., in qualitative conformity with the former lines.

In the region I of the phase equilibrium diagram the grain-boundary segregations are formed without precipitation of phases. In region II precipitation of the grain-boundary phase becomes possible, e.g., in the region of triple joints of grains. In region III, discontinuous decomposition similar to the spinodal decomposition occurs at GBs. Heterogeneous nucleation in the volume of grains becomes possible in region IV (e.g., at dislocations). Finally, spinodal decomposition both in the volume and at the grain boundaries proceeds in region V. The characteristic precipitate morphologies (the central column in Fig. 7) are obtained via phase-field simulations, here-with the configuration of grains with two triple joints is considered. The main features of the alloy's behavior are completely reproduced in the phase-field simulation, but the role of the pseudospinodal line is played by a classic spinodal line.

As can be seen from a comparison of Figs. 7a and 7b, the $c_b^e(T)$ and $c_b^{ps}(T)$ lines in large grains differ little

from their analog $c_{\text{inf}}^e(T)$, $c_{\text{inf}}^{ps}(T)$ in an infinite medium. In contrast, decomposition in the grain volume is greatly suppressed for small grains, which corresponds to the strong shift of these lines downward and to the right in the diagram.

CONCLUSIONS

A set of algebraic equations was proposed for describing segregations and grain-boundary decomposition taking into account finite grain size. It was shown that in dilute solid solutions both grain-boundary decomposition and decomposition in a grain volume are substantially suppressed in the nanocrystalline state. A generalized phase-equilibrium diagram was constructed, and a classification for the morphology of precipitates that considers the impurity segregations at grain boundaries and grain-boundary decomposition was proposed.

ACKNOWLEDGMENTS

This study was performed within the framework of the state task (“Magnit,” no. AAAA-A18-118020290129-5).

REFERENCES

1. Y. Li, A. J. Bushby, and D. J. Dunstan, *Proc. R. Soc. London, Ser. A* **472**, 20150890 (2016).
2. J. W. Morris, in *Proceedings of the International Symposium of Ultrafine Grained Steels*, Ed. by S. Takaki and T. Maki (Iron Steel Inst., Tokyo, Japan, 2001), p. 34.
3. H. Gao, B. Ji, I. L. Jager, et al., *Proc. Natl. Acad. Sci.* **100**, 5597 (2003).
4. R. Z. Valiev and I. V. Aleksandrov, *Nanostructured Materials Produced by Severe Plastic Deformation* (Logos, Moscow, 2000) [in Russian].
5. H. Yu, M. Yan, C. Lu, et al., *Sci. Rep.* **6**, 36810 (2016).
6. J. Tianfu et al., *Mater. Sci. Eng. A* **432**, 216 (2006).
7. R. D. K. Misra et al., *Acta Mater.* **84**, 339 (2015).
8. D. M. Field and D. C. van Aken, *Metall. Mater. Trans. A* **47**, 1912 (2016).
9. R. Z. Valiev, N. A. Enikeev, and T. G. Langdon, *Kovove Mater.* **49**, 1 (2011).
10. R. Z. Valiev, *Nat. Mater.* **12**, 289 (2013).
11. *Nanostructured Metals and Alloys: Processing, Microstructure, Mechanical Properties, and Applications*, Ed. by S. H. Whang (Elsevier, Amsterdam, 2011).
12. Yu. N. Gornostyrev, I. K. Razumov, and A. Ye. Yermakov, *J. Mater. Sci.* **39**, 5003 (2004).
13. *Metals and Alloys, The Handbook* (Professional, Mir Sem'ya, St. Petersburg, 2003) [in Russian].
14. M. I. Gol'dshtein, V. V. Popov, and A. E. Aksel'rod, *Izv. Akad. Nauk SSSR, Met.*, No. 2, 93 (1986).
15. T. Chandra, N. Wanderka, W. Reimers, and M. Ionescu, *Mater. Sci. Forum* **638**, 3388 (2010).
16. Y. I. Hai-Iong, D. U. Lin-Xiu, et al., *J. Iron Steel Res., Int.* **16** (4), 72 (2009).
17. I. K. Razumov, *Russ. J. Phys. Chem. A* **88**, 494 (2014).
18. J. Christian, *The Theory of Transformations in Metals and Alloys (Equilibrium and General Kinetic Theory)* (Pergamon, Oxford, 1975).
19. R. H. Fowler and E. A. Guggenheim, *Statistical Thermodynamics* (Cambridge Univ. Press, Cambridge, 1939).
20. K. Ishida, *J. Alloys Compd.* **235**, 244 (1996).
21. A. A. Mirzoev, M. M. Yalalov, and D. A. Mirzaev, *Phys. Met. Metallogr.* **101**, 341 (2006).
22. A. A. Mirzoev, M. M. Yalalov, and D. A. Mirzaev, *Phys. Met. Metallogr.* **103**, 83 (2007).
23. A. A. Mirzoev, M. M. Yalalov, D. A. Mirzaev, and K. Yu. Okishev, *Phys. Met. Metallogr.* **114**, 1 (2013).
24. A. G. Khachaturyan, *The Theory of Phase Transformations and Structure of Solid Solutions* (Nauka, Moscow, 1974) [in Russian].
25. J. W. Cahn and J. E. Hilliard, *J. Chem. Phys.* **28**, 258 (1958).
26. I. K. Razumov, Yu. N. Gornostyrev, and A. Ye. Yermakov, *J. Alloys Compd.* **434–435**, 535 (2007).
27. K. Binder, *Phys. Rev. A* **29**, 341 (1984).
28. I. K. Razumov, *Phys. Solid State* **59**, 639 (2017).
29. I. N. Kar'kin, L. E. Kar'kina, P. A. Korzhavyi, and Yu. N. Gornostyrev, *Phys. Solid State* **59**, 106 (2017).
30. I. G. Shmakov, I. K. Razumov, O. I. Gorbatov, Yu. N. Gornostyrev, and P. A. Korzhavyi, *JETP Lett.* **103**, 112 (2016).

Translated by O. Kadkin